Analysis of the Optimum Gain of a High-Pass L-Matching Network for Rectennas

Manel Gasulla [1],* , Josep Jordana [1], Francesc-Josep Robert [1] and Jordi Berenguer [2]

[1] e-CAT Reasearch Group, Department of Electronic Engineering,
Castelldefels School of Telecommunications and Aerospace Engineering, Universitat Politècnica de Catalunya, c/Esteve Terradas, 7, 08860 Castelldefels (Barcelona), Spain; jose.jordana@upc.edu (J.J.); francesc.j.robert@upc.edu (F.-J.R.)

[2] CSC Research Group, Department of Signal Theory and Communications, Castelldefels School of Telecommunications and Aerospace Engineering, Universitat Politècnica de Catalunya, c/Esteve Terradas, 7, 08860 Castelldefels (Barcelona), Spain; jordi.berenguer@upc.edu

* Correspondence: manel.gasulla@upc.edu; Tel.: +34-934-137-092

Abstract: Rectennas, which mainly consist of an antenna, matching network, and rectifier, are used to harvest radiofrequency energy in order to power tiny sensor nodes, e.g., the nodes of the Internet of Things. This paper demonstrates for the first time, the existence of an optimum voltage gain for high-pass L-matching networks used in rectennas by deriving an analytical expression. The optimum gain is that which leads to maximum power efficiency of the rectenna. Here, apart from the L-matching network, a Schottky single-diode rectifier was used for the rectenna, which was optimized at 868 MHz for a power range from −30 dBm to −10 dBm. As the theoretical expression depends on parameters not very well-known a priori, an accurate search of the optimum gain for each power level was performed via simulations. Experimental results show remarkable power efficiencies ranging from 16% at −30 dBm to 55% at −10 dBm, which are for almost all the tested power levels the highest published in the literature for similar designs.

1. Introduction

Radio frequency (RF) energy harvesting has been widely proposed to power tiny devices such as RFID tags, autonomous sensors, or IoT (Internet of Things) nodes [1–9]. RF energy can be harvested either from dedicated sources, such as in the case of RFID devices, or from the RF energy already present in the ambient and coming from unintentional sources such as TV, FM radio, cellular, or WiFi emitters.

In order to harvest RF energy, a rectenna (rectifying antenna) is used. Figure 1 shows the block diagram of a conventional rectenna, consisting of an antenna, an impedance matching network and a rectifier. The rectifier provides a suitable DC voltage in order to power a load, e.g., an RFID tag or IoT node, and the matching network matches the output impedance of the antenna to the equivalent impedance at the input of the rectifier in order to transfer the available maximum power.

As the available power at the antenna decreases so does the generated voltage. Whenever this voltage is not high enough to properly bias the diodes of the rectifier, the power efficiency decreases severely. Several techniques have been proposed in order to increase the efficiency at low power levels. For example, in [1,2,10] dual-stage solutions were proposed, where each of the two implemented circuits was optimized for different ranges of input power. In [11], the size of the diode-connected MOS transistors was optimized. On the other hand, in order to reduce the voltage drop of the diodes,

novel devices have been proposed such as MOS floating-gate devices [12], tunnel FETs [13], or MOS transistors with a new bulk connection [14]. Another widely used technique consists in using the matching network for boosting the voltage at the rectifier input [4,8,14–26]. Among them, one of the simplest and most widely used is the L-matching network, where the voltage gain is fixed by the resistance value of the load.
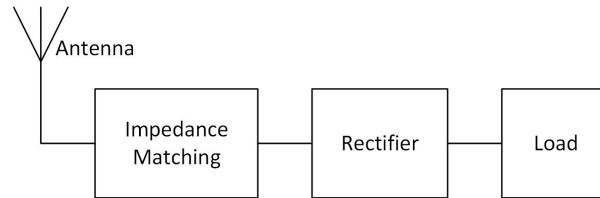

Figure 1. Block diagram of a rectenna with an output load.

This paper demonstrates for the first time the existence of an optimum voltage gain for a high-pass L-matching network used in rectennas by deriving an analytical expression. The optimum gain is that which leads to maximum power efficiency of the rectenna. As the focus is on the matching network, a rectifier with a single series diode configuration was selected for simplicity. Input power levels in the range of -30 dBm to -10 dBm at the 868 MHz Short Range Devices (SRD) band were considered. At each power level, the value provided by the expression of the optimum gain was used as the initial point for an ensuing accurate search via simulations. The rectenna was later implemented and experimental results show remarkable power efficiencies compared with other works with similar designs found in the literature.

The paper is organized as follows: Section 2 presents a theoretical analysis of the rectenna where the analytical expression of the optimum voltage gain of the matching network is derived. Section 3 shows simulation results of the rectenna with the Keysight ADS software for obtaining the optimum gain and components of the matching network that will be used in the implementation of the circuit. In Section 4 the performance of the implemented rectenna is presented. Section 5 concludes the work and two appendices present supplemental material.

2. Theoretical Analysis of the Rectenna

This section presents the analysis of the rectenna with both an ideal (Section 2.1) and a lossy (Section 2.2) matching network. The optimum voltage gain of the matching network is derived in Section 2.2.

2.1. Rectenna with Ideal Matching Network

Figure 2 shows the circuit schematic of the proposed rectenna, which includes a high pass L-matching network (composed of a capacitor C_m and an inductor L_m), a half-wave rectifier and an output filtering capacitor (C_o) and load (R_o). The antenna is modelled by a sinusoidal voltage source v_a with a series radiation resistance R_a. On the other hand, v_{in}, Z_{in} and P_{in} respectively are the voltage, impedance and power at the input of the rectifier, and V_o and P_o respectively are the DC voltage and power at the load.
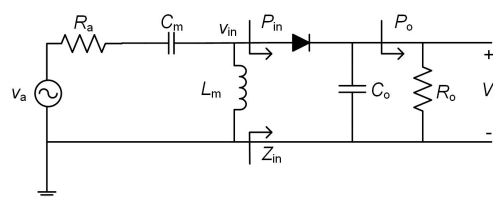

Figure 2. Proposed rectenna.

The voltage amplitude (or peak voltage) of v_a is given by [17]:

$$V_{ap} = 2\sqrt{2R_a P_{av}}, \tag{1}$$

where P_{av} is the available power at the antenna. On the other hand, the overall power efficiency of the rectenna is defined as:

$$\eta_{rect} = \eta_{in}\eta_o, \tag{2}$$

where the input efficiency is given by:

$$\eta_{in} = \frac{P_{in}}{P_{av}}, \tag{3}$$

and the rectifier efficiency is:

$$\eta_o = \frac{P_o}{P_{in}} = 1 - \frac{V_\gamma}{V_{inp}}, \tag{4}$$

being V_{inp} the amplitude voltage of v_{in} and V_γ the threshold forward voltage of the diode (assumed constant here). Equation (4) is a simplistic approximation that neglects all the parasitic components and non idealities of the diode except V_γ.

In order to achieve a high value of η_{in} (ideally 1), Z_{in} has to be matched to R_a. On the other hand, from Equation (4), lower values of V_γ and higher values of V_{inp} lead to a higher value of η_o. Thus, η_o can be increased, for example, by using Schottky diodes (low V_γ) and a matching network with a high voltage gain (high V_{inp}). In order to illustrate how the matching network provides this gain, the circuit of Figure 2 is transformed into the circuit of Figure 3, where C_{in} and R_{in} model Z_{in} in Figure 2.
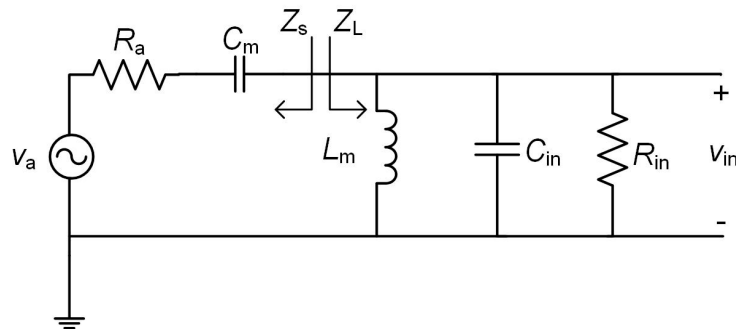

Figure 3. Equivalent circuit of the rectenna.

C_{in} is mainly due to the parasitic capacitance of the diode whenever C_o is much larger, which is usually the case, and R_{in}, which models the power delivered to the rectifier input, is given by [27]:

$$R_{in} = \frac{R_o}{2} \frac{1}{1 - V_\gamma/V_{inp}}. \tag{5}$$

In order to transfer the maximum power to the rectifier input ($P_{in} = P_{av}$ and thus $\eta_{in} = 1$), it must be accomplished that $Z_L = Z_s^*$, resulting in the following voltage gain of the matching network:

$$G_t = \frac{V_{inp}}{V_{ap}} = \frac{1}{2}\sqrt{\frac{R_{in}}{R_a}} = \frac{1}{2}\sqrt{(1 + Q^2)}, \tag{6}$$

where Q is the quality factor of the circuit. Appendix A shows the resulting expressions for C_m and L_m as well graphs of these parameters in function of G_t.

As can be seen from Equation (6), G_t depends on the relationship between R_{in} and R_a, so the gain G_t can be made arbitrarily large by increasing R_{in}. Expression (6) can also be derived equating the power at the input of the matching network with that dissipated in R_{in}, assuming a lossless matching

network [16]. Thus, an increase of R_{in} requires a square increase of v_{in} (and thus of G_t) to keep power constant. On the other hand, R_{in} can be increased, from Equation (5), by increasing R_o. However, R_o is a priori fixed by the load to be powered, e.g., an IoT node. Fortunately, R_o can be arbitrarily and automatically changed by placing an additional impedance matching stage between the rectenna output and the load. Such stage, which is out of the scope of this work, is normally implemented by a maximum power point tracker, which has been extensively used in solar, thermal, and mechanical energy harvesters, but also in RF harvesters, such as in [28–30].

2.2. Rectenna with Lossy Matching Network: Optimum Voltage Gain

In the previous analysis, the losses of the matching network components have not been considered and thus will be taken into account next. As will be shown, their inclusion is significant and leads to the concept of optimum voltage gain of the matching network.

In general, the parasitic loss of capacitors is very small compared with that of inductors [16,31,32] and will be neglected in the analysis. Then, taking into account the inductor model of Appendix B, Figure 3 is transformed into Figure 4, where $L_m \approx L'_m$ and C_{in} and R_{in} have been substituted by C_e and R_e. The resistance R_e includes the parasitic losses (R_p) of the coil and is given by:

$$\frac{1}{R_e} = \frac{1}{R_p} + \frac{1}{R_{in}}, \tag{7}$$

being:

$$\frac{1}{R_p} = \frac{1}{R'_v} + \frac{1}{R'_1}, \tag{8}$$

and C_e includes the parasitic capacitance of the coil and is given by:
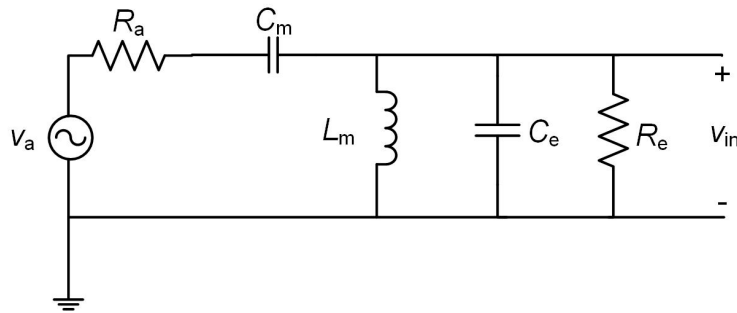
$$C_e = C_{in} + C'_1, \tag{9}$$

Figure 4. Equivalent circuit of the rectenna taking into account the inductor model of Figure A4 with R_2 neglected.

For the circuit of Figure 4, the gain of the matching lossy network is:

$$G_t = \frac{1}{2}\sqrt{\frac{R_e}{R_a}}, \tag{10}$$

Now, even with a large value of R_{in}, R_e and thus G_t will be limited by R_p. Further, at matching conditions [16]:

$$\eta_{in} = \frac{R_e}{R_{in}} = \frac{R_p}{R_p + R_{in}}, \tag{11}$$

as some power will be dissipated at R_p. Therefore, large values of R_{in} ($>>R_p$ and thus $>>R_e$) decrease η_{in} without significantly increasing G_t and thus η_o. Contrariwise, low values of R_{in} ($<<R_p$ and thus

$R_\text{in} \approx R_\text{e}$) decrease G_t and thus η_o without significantly increasing η_in (≈ 1). So, a trade-off exists for achieving a maximum value of η_rect, which leads to an optimum R_in and G_t.

The optimum value of G_t can be found by expressing Equation (2) in function of G_t, equating its derivative to zero and finding the roots. First, operating from Equations (7) and (10), we obtain

$$R_\text{in} = \frac{4G_\text{t}^2 R_\text{a} R_\text{p}}{R_\text{p} - 4G_\text{t}^2 R_\text{a}}, \tag{12}$$

and substituting this in Equation (11) we get:

$$\eta_\text{in} = 1 - 4G_\text{t}^2 \frac{R_\text{a}}{R_\text{p}}, \tag{13}$$

On the other hand, using Equation (6) in Equation (4) we arrive at:

$$\eta_\text{o} = 1 - \frac{V_\gamma}{G_\text{t} V_\text{ap}}, \tag{14}$$

and thus from Equations (2), (13) and (14) we obtain:

$$\eta_\text{rect} = \left(1 - 4G_\text{t}^2 \frac{R_\text{a}}{R_\text{p}}\right)\left(1 - \frac{V_\gamma}{G_\text{t} V_\text{ap}}\right), \tag{15}$$

Figure 5 shows a qualitative representation of Equations (13)–(15). As can be seen, η_in decreases and η_o increases with increasing values of G_t, leading to an optimum value of G_t ($G_\text{t,opt}$) that provides the maximum value of η_rect (η_max).
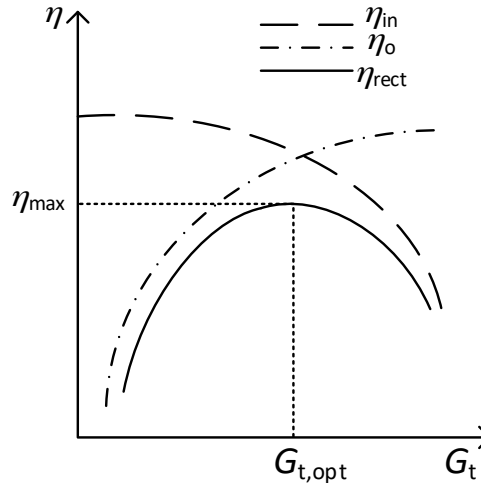

Figure 5. Qualitative graphs of the efficiencies of the rectenna versus G_t.

The expression of $G_\text{t,opt}$ can be reached by doing the derivative of Equation (15) with respect to G_t and equating to zero, thus arriving to the following third-degree equation:

$$G_\text{t}^3 - \frac{V_\gamma}{2V_\text{ap}}G_\text{t}^2 - \frac{R_p V_\gamma}{8 R_a V_\text{ap}} = 0. \tag{16}$$

In this case, only a single positive real root results, which can be approximated to:

$$G_\text{t,opt} \approx \frac{1}{6}\frac{V_\gamma}{V_\text{ap}} + \frac{1}{2}\sqrt[3]{\frac{V_\gamma}{V_\text{ap}}\frac{R_\text{p}}{R_\text{a}}}, \tag{17}$$

The derivation and expression for $G_{\mathrm{t,opt}}$ has not previously reported in the literature. As can be seen, $G_{\mathrm{t,opt}}$ increases with increasing values of R_{p} and V_{γ} and with decreasing values of V_{ap}. This can be also inferred from the above expressions and Figure 5. Effectively, from Equation (13), an increase of R_{p} (decrease of inductor losses) increases η_{in}, shifting upwards the corresponding curve in Figure 5 and thus to the right $G_{\mathrm{t,opt}}$ (higher value). At the same time, the value of η_{max} will increase. On the other hand, from Equation (14), a higher value of V_{γ} or a lower value of V_{ap} decrease η_{o}, shifting downwards the corresponding curve in Figure 5 and thus again to the right $G_{\mathrm{t,opt}}$. In this case, though, η_{max} will decrease. So, η_{max} increases with increasing values of R_{p} and V_{ap} and with decreasing values of V_{γ}.

In order to obtain Equation (17), the values of V_{γ} and R_{p} are required. However, V_{γ} depends on the current flowing through the diode, which depends on P_{av} but also on G_{t}. On the other hand, R_{p} depends on the specific commercial component of L_{m}, whose value, from Equation (A6), again depends on G_{t}. Therefore, it is not straightforward obtaining $G_{\mathrm{t,opt}}$ and it will be found here by simulations, as shown in Section 3. Anyhow, the above derivation demonstrates the existence of an optimum gain value, provides more insight on the optimum gain and rectenna efficiency, and from Equation (17) an initial guess can be used for the simulations.

3. Rectenna Simulation Analysis

Simulations of the rectenna of Figure 2 have been carried out using the Keysight ADS software. The Harmonic Balance Analysis was used in order to compute the steady state solutions. For the diode, a Schottky HSMS-2850 device (Avago Technologies, Sant Jose, CA, USA) was selected, as it presents a low voltage drop ($V_{\gamma} \approx 0.1$ V @ 0.1 mA) and a low capacitance ($C_{\mathrm{jo}} = 0.18$ pF). Input power levels from -30 dBm to -10 dBm in steps of 5 dBm were used at a frequency of 868 MHz. Commercial components from the vendor libraries for C_{m} (AVX, Fountain Inn, SC, USA) and L_{m} (Coilcraft, Cary, IL, USA) were also used. A layout was also included in the simulations and the Momentum simulator was executed in order to obtain the related S-parameters. The physical dimensions of the printed circuit board (PCB) were 30.75 mm long and 12.10 mm width. Figure 6 shows the layout of the PCB, with indications to the placement of the components. The parameters of a Rogers substrate (RO4003C, Rogers, Chandler, AZ, USA) were selected ($\varepsilon_{\mathrm{r}} = 3.55$, $\tan\delta = 0.0021$, thickness = 1.524 mm).
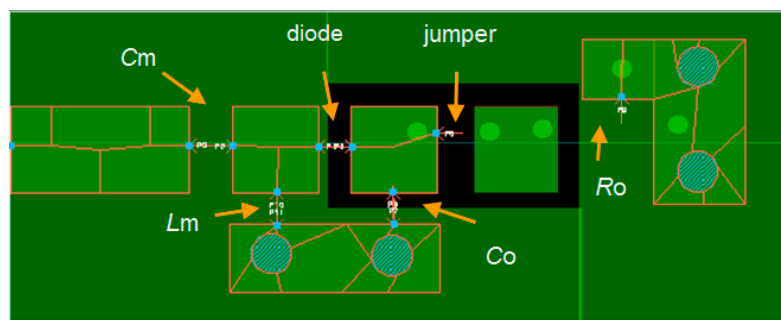

Figure 6. PCB Layout of the rectenna with indication to the placement of the components.

In order to find $G_{\mathrm{t,opt}}$ for each specific power level (P_{av}), the following procedure was followed. First, an initial value of G_{t} is calculated using Equation (17) with appropriate values of V_{γ} and R_{p}. From Equation (A5), the corresponding value of C_{m} is calculated and the component with the nearer commercial value is selected. Then, an appropriate component value of L_{m} is selected and a sweep of η_{rect} over R_{o} is performed. The procedure is repeated for several values of L_{m} until finding the curve with the maximum efficiency. In order to better illustrate the implemented procedure, Figure 7 shows the case for $P_{\mathrm{av}} = -10$ dBm and $C_{\mathrm{m}} = 0.5$ pF ($G_{\mathrm{t}} = 3.7$). As can be seen, there is a maximum value of η_{rect} (around 55%) for $L_{\mathrm{m}} = 27$ nH and $R_{\mathrm{o}} = 4$ kΩ. These parameters values are saved and the

whole procedure is repeated for different values of C_m (and thus of G_t). Figure 8 shows the attained maximum efficiencies for $P_{av} = -10$ dBm for each one of the selected values of C_m (or G_t). As can be seen, the maximum efficiency (η_{max}) at -10 dBm was achieved for $G_t = 3.7$ ($C_m = 0.5$ pF, the case represented in Figure 7). Finally, the whole process is repeated for the different input power levels.
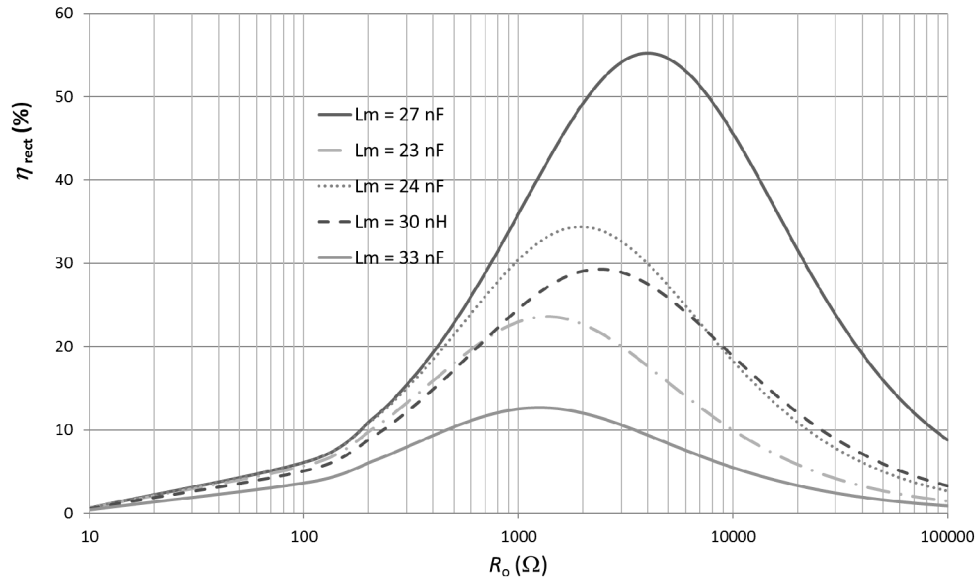

Figure 7. Simulation results of η_{rect} versus R_o for several values of L_m at $C_m = 0.5$ pF ($G_t = 3.7$) and $P_{av} = -10$ dBm.
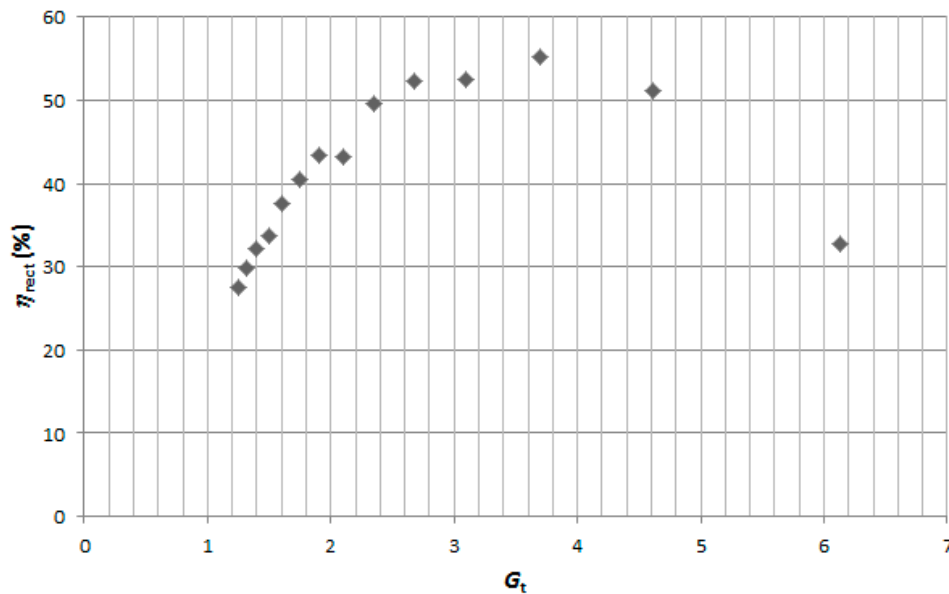

Figure 8. Simulation results of η_{rect} for several values of G_t at $P_{av} = -10$ dBm. A maximum value (η_{max}) of 55.2% was achieved at $G_t = 3.7$ ($C_m = 0.5$ pF).

Table 1 summarizes the results of the simulations showing η_{max} along with the optimal values of G_t, C_m, L_m, R_o, and V_o for each one of the selected power levels (P_{av}). As can be seen, the optimum value of G_t increases and η_{max} decreases with a decreasing value of P_{av} and thus of V_{ap}, which agrees with the discussion of Section 2.2. As a numerical example, the value of $G_{t,opt}$ for -20 dBm is calculated using Equation (17). Taking the data of the 27 nH inductor from Appendix B, it can

be found from Equation (8) that R_p is 12.6 kΩ. Then, assuming a value of V_γ = 0.1 V, $G_{t,opt}$ = 3.94 results (C_m = 0.47 pF). The value of C_m shown in Table 1 (0.5 pF) is in fact the nearest commercial value available from the vendor library.

Table 1. Values of η_{max} along with the optimal values of G_t, C_m, L_m, R_o and V_o.

P_{av} (dBm)	η_{max} (%)	G_t	C_m (pF)	L_m (nH)	R_o (kΩ)	V_o (mV)
−30	10.9	5.48	0.3	30	8.6	30.7
−25	18.6	5.48	0.3	30	7.0	64.2
−20	30.8	3.70	0.5	27	4.6	119
−15	44.6	3.70	0.5	27	4.4	249
−10	55.2	3.70	0.5	27	4.0	470

4. Experimental Results and Discussion

The PCB layout of Figure 6 was produced and C_m = 0.5 pF, L_m = 27 nH, and C_o = 1 nF were used. The selected values of C_m and L_m lead to G_t = 3.7 and match that of P_{av} = −20 dBm, −15 dBm and −10 dBm in Table 1. In order to choose an appropriate frequency for the experimental tests, the input reflection coefficient S_{11} of the rectenna was measured for P_{av} from −30 dBm to −10 dBm in steps of 5 dBm using for R_o the corresponding values of Table 1. Results are shown in Figure 9.
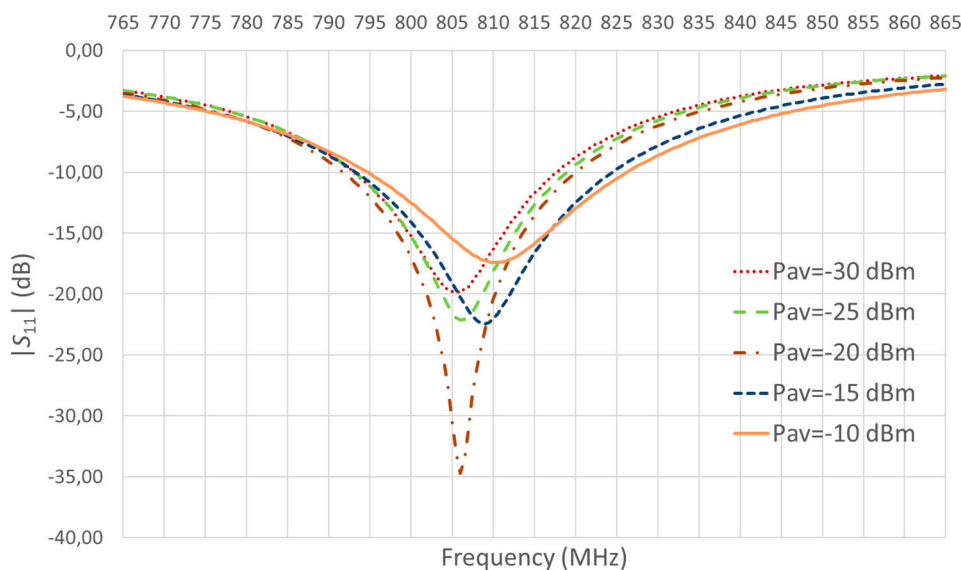

Figure 9. Experimental results of $|S_{11}|$ for different power levels.

As can be seen, there is a deviation of the frequencies at which the minimum value is achieved with respect to the theoretical frequency of 868 MHz used in the simulations. This is probably due to differences between the models of the components used in the simulations and their actual values. The tolerance of the network components and deviations of the parasitic capacitances of the inductor and diode can be the main cause. In addition, the capacitance of the diode is nonlinear with the diode voltage drop and thus with v_{in}, which accounts for the frequency shift down as the power decreases [8]. On the other hand, Table 2 shows the values of the input impedance of the rectenna at a frequency of 814 MHz, which was the value selected for the rest of tests. As can be seen, values approach the value of R_a = 50 Ω and, from Figure 9, $|S_{11}|$ was lower than −10 dB at that frequency for all power levels.

Table 2. Values of the input impedance of the rectenna at 814 MHz using for R_o the values of Table 1 .

P_{av} (dBm)	−30	−25	−20	−15	−10
Impedance (Ω)	67.3 + j22.4	65.9 + j18.8	59.6 + j10.7	60.7 − j9.9	62.3 − j11.7

An RF signal generator was used at the input of the harvester to emulate the antenna and to generate different values of P_{av}. Output power (P_o) was measured by means of a Source Measurement Unit (SMU, B2901, Agilent, Santa Rosa, CA, USA). The frequency of the RF signal generator was set to 814 MHz, as previously stated, since it provided a relative high output power at all values of P_{av}. Anyhow, other nearby frequencies (with a difference of few units of megahertz, e.g., 810 MHz or 805 MHz) could have been chosen without significant changes in P_o.

While measuring P_o, the SMU fixed the output voltage (V_o) and this voltage was manually swept until the maximum value of P_o ($P_{o,max}$) was obtained. Maximum efficiency (η_{max}) was estimated as $P_{o,max}$ divided by P_{av}. Then, the equivalent value of R_o was estimated from V_o and $P_{o,max}$. This procedure was faster than using a trimmer for R_o and estimating P_o from the measurements of R_o and V_o until $P_{o,max}$ was obtained. Table 3 shows the values of η_{max}, R_o, and V_o. Values are similar to that of the simulations (Table 1). Efficiencies range from 15.7% at −30 dBm to 55.2% at −10 dBm.

Table 3. Experimental results of η_{max}, R_o, and V_o.

P_{av} (dBm)	η_{max} (%)	R_o (kΩ)	V_o (mV)
−30	15.7	5.7	30
−25	24.6	4.6	60
−20	36.0	4.7	130
−15	47.2	4.5	260
−10	55.2	4.5	500

Table 4 shows a comparative of the rectenna efficiency (in percentage) of this work with other papers using similar designs. Some of the values are imprecise as they were inferred from graphs. All of them use a matching network (in most cases an L-type) and the same model of diode (except in [10] that use an HSMS-282X model (Avago Technologies). The frequency was similar (in the range of 850 MHz to 950 MHz) except in [10] (2.45 GHz), [20] (434 MHz), and [33] (1.8 GHz). As can be seen, this work outperforms the results of the rest of papers except at −30 dBm, where [20] presents a higher efficiency. It is possible that the losses of the inductor used here, which limit the network gain and efficiency, are higher than those of the inductor used in [20] (details of the commercial inductor not provided).

Table 4. Comparative of the rectenna efficiency (%) of this work with other papers with similar designs.

P_{av} (dBm)	This Work	[1]	[2]	[8]	[10]	[20]	[33]	[34]
−30	16	-	-	-	-	22	5	-
−25	25	-	-	20	-	-	8	-
−20	36	2	10	33	-	35	15	-
−15	47	5	20	42	-	-	25	30
−10	55	10	35	51	15	47	35	35

5. Conclusions

This work has demonstrated the existence of an optimum voltage gain for L-matching networks used in rectennas by providing an analytical expression. The rectenna, which also includes a Schottky single-diode rectifier, has been optimized at 868 MHz for a power range from −30 dBm to −10 dBm. As not all the parameters of the expression are well known a priori, an accurate search of the gain has

been performed by simulations. Furthermore, a prototype has been implemented with experimental results showing remarkable power efficiencies, ranging from 16% at −30 dBm to 55% at −10 dBm. These results are amongst the highest published in the literature for similar designs.

Author Contributions: Manel Gasulla performed the theoretical analysis and jointly with Josep Jordana conceived and designed the experiments, and wrote the paper; Josep Jordana performed the simulations, implementation and experiments of the rectenna; Jordi Berenguer performed the measurements of the return loss and input impedance of the rectenna; Francesc-Josep Robert supported to Josep Jordana and Jordi Berenguer on the experiments and measurements.

Conflicts of Interest: The authors declare no conflict of interest. The founding sponsors had no role in the design of the study; in the collection, analyses, or interpretation of data; in the writing of the manuscript, and in the decision to publish the results.

Appendix A. Expressions for C_m and L_m and Corresponding Graphs

This appendix provides the expressions for C_m and L_m of the matching network along with graphs of these parameters.

In order to transfer the maximum power to the rectifier input, it must be accomplished that $Z_L = Z_s^*$ in Figure 3, where:

$$Z_s = R_a + \frac{1}{j\omega C_m}, \tag{A1}$$

$$\frac{1}{Z_L} = \frac{1}{R_{in}} + j\omega C_{in} + \frac{1}{j\omega L_m}, \tag{A2}$$

being ω the angular frequency. Operating, we obtain:

$$C_m = \frac{1}{\omega \sqrt{R_a(R_{in} - R_a)}}, \tag{A3}$$

$$L_m = \frac{1}{\omega^2 C_{in} + \omega^2 C_m \frac{R_{in} - R_a}{R_{in}}}, \tag{A4}$$

and the gain given by Equation (6). The parameters L_m and C_m can also be expressed in function of G_t and Q as:

$$C_m = \frac{1}{\omega R_a \sqrt{4\,G_t^2 - 1}} = \frac{1}{\omega R_a Q}, \tag{A5}$$

$$L_m = \frac{4\,G_t^2\,R_a}{\omega \sqrt{4\,G_t^2 - 1} + 4\,G_t^2\,R_a\,C_{in}\,\omega^2} = \frac{1}{\omega^2}\frac{1}{C_{in} + C_m Q^2/(1 + Q^2)}. \tag{A6}$$

Figures A1 and A2 show the values of C_m and L_m as a function of G_t for R_a = 50 Ω, respectively. As for the calculus of L_m, two different cases have been considered, C_{in} equal to 0 pF and to 0.18 pF. The value of 0.18 pF emulates the input capacitance of the selected diode (HSMS-2850) for the rectenna (Sections 3 and 4). C_m is inversely proportional to G_t (strictly only for $G_t \gg 1$) and Q. On the other hand, L_m is inversely proportional to C_m (so, proportional to G_t and Q) for C_{in} = 0 but for C_{in} = 0.18 pF saturates to $1/(\omega^2 C_{in})$ with G_t (or Q) increasing (C_m decreasing).
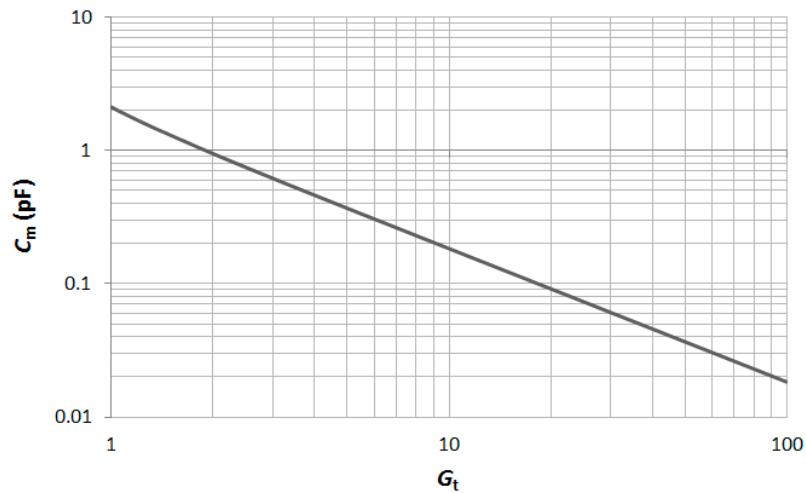
Figure A1. C_m values in function of G_t.
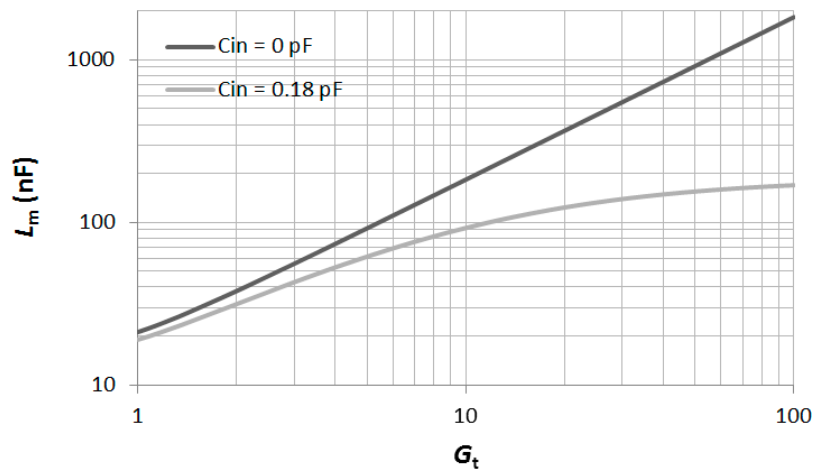

Figure A2. L_m values in function of G_t for C_in = 0 pF and C_in = 0.18 pF.

Appendix B. Lumped Model of the Inductor Including Parasitic Effects

Figure A3 shows the lumped model of the Coilcraft RF surface mount inductor used in the implementation of the circuit of Figure 2. The value of the frequency-dependent variable resistor R_v relates to the skin effect and is calculated from $R_\mathrm{v} = k' \sqrt{f}$, where f is the operation frequency and k' is a constant that depends on the nominal value of the inductance.
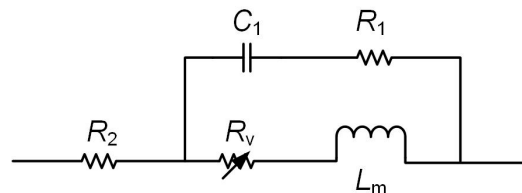

Figure A3. Equivalent lumped element model of the inductor.

Using the series to parallel equivalent circuit transformation for the two branches of Figure A3 the equivalent circuit of Figure A4 results.
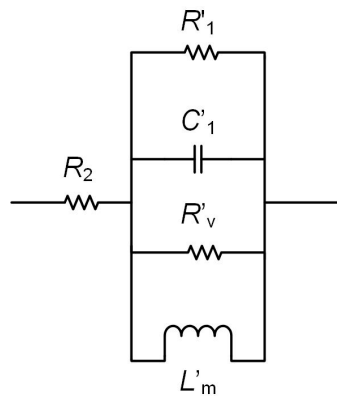
Figure A4. Parallel equivalent circuit of the inductor of Figure A3.

The value of the components of the circuit of Figure A4 respect to those of the circuit of Figure A3 are given by the following expressions:

$$R'_1 = R_1 \frac{R_1^2 C_1^2 \omega^2 + 1}{R_1^2 C_1^2 \omega^2}, \tag{A7}$$

$$C'_1 = \frac{C_1}{R_1^2 C_1^2 \omega^2 + 1}, \tag{A8}$$

$$L'_m = L_m \left(1 + \left(\frac{R_v}{\omega L_m} \right)^2 \right), \tag{A9}$$

$$R'_v = R_v \left(1 + \left(\frac{\omega L}{R_v} \right)^2 \right). \tag{A10}$$

The model of Figure A4 is substituted in the circuit of Figure 3, resulting in the circuit of Figure 4, where the value of R_2 has been neglected as it usually is very small. As an example, the 27 nH inductor used in the implemented matching network (Section 4) has the following parameters: $R_1 = 17\ \Omega$, $R_2 = 30\ \text{m}\Omega$, $C_1 = 49\ \text{fF}$, $L_m = 27\ \text{nH}$, $k' = 5.75 \times 10^{-5}$. At 868 MHz the value of the parallel components of Figure A4 are: $R'_1 = 824\ \text{k}\Omega$, $C'_1 = 49\ \text{fF}$, $R'_v = 12.8\ \text{k}\Omega$, $L'_m = 27\ \text{nH}$.

References

1. Nintanavongsa, P.; Muncuk, U.; Lewis, D.R.; Chowdhury, K.R. Design Optimization and Implementation for RF Energy Harvesting Circuits. *IEEE J. Emerg. Sel. Top. Circuits Syst.* **2012**, *2*, 24–33. [CrossRef]
2. Di Marco, P.; Stornelli, V.; Ferri, G.; Pantoli, L.; Leoni, A. Dual band harvester architecture for autonomous remote sensors. *Sens. Actuators A Phys.* **2016**, *247*, 598–603. [CrossRef]
3. Shaker, G.; Chen, R.; Milligan, B.; Qu, T. Ambient electromagnetic energy harvesting system for on-body sensors. *Electron. Lett.* **2016**, *52*, 1834–1836. [CrossRef]
4. Attaran, A.; Rashidzadeh, R.; Muscedere, R. Chipless RFID tag using RF MEMS switch. *Electron. Lett.* **2014**, *50*, 1720–1722. [CrossRef]
5. Talla, V.; Kellogg, B.; Ransford, B.; Naderiparizi, S.; Gollakota, S.; Smith, J.R. Powering the Next Billion Devices with Wi-Fi. *Commun. ACM* **2015**, *60*, 83–92. [CrossRef]
6. Pinuela, M.; Mitcheson, P.D.; Lucyszyn, S. Ambient RF Energy Harvesting in Urban and Semi-Urban Environments. *IEEE Trans. Microw. Theory Tech.* **2013**, *61*, 2715–2726. [CrossRef]
7. Kaushik, K.; Mishra, D.; De, S.; Chowdhury, K.R.; Heinzelman, W. Low-Cost Wake-Up Receiver for RF Energy Harvesting Wireless Sensor Networks. *IEEE Sens. J.* **2016**, *16*, 6270–6278. [CrossRef]
8. Singh, G.; Ponnaganti, R.; Prabhakar, T.V.; Vinoy, K.J. A tuned rectifier for RF energy harvesting from ambient radiations. *AEU Int. J. Electron. Commun.* **2013**, *67*, 564–569. [CrossRef]

9. Sample, A.; Smith, J.R. Experimental results with two wireless power transfer systems. In Proceedings of the 2009 IEEE Radio and Wireless Symposium, San Diego, CA, USA, 18–22 January 2009; IEEE: New York, NY, USA, 2009; pp. 16–18.

10. Mirzavand, F.; Nayyeri, V.; Soleimani, M.; Mirzavand, R. Efficiency improvement of WPT system using inexpensive auto-adaptive impedance matching. *Electron. Lett.* **2016**, *52*, 2055–2057. [CrossRef]

11. Yi, J.; Ki, W.-H.; Tsui, C.-Y. Analysis and Design Strategy of UHF Micro-Power CMOS Rectifiers for Micro-Sensor and RFID Applications. *IEEE Trans. Circuits Syst. I Regul. Pap.* **2007**, *54*, 153–166. [CrossRef]

12. Le, T.; Mayaram, K.; Fiez, T. Efficient Far-Field Radio Frequency Energy Harvesting for Passively Powered Sensor Networks. *IEEE J. Solid-State Circuits* **2008**, *43*, 1287–1302. [CrossRef]

13. Liu, H.; Li, X.; Vaddi, R.; Ma, K.; Datta, S.; Narayanan, V. Tunnel FET RF Rectifier Design for Energy Harvesting Applications. *IEEE J. Emerg. Sel. Top. Circuits Syst.* **2014**, *4*, 400–411. [CrossRef]

14. Shokrani, M.R.; Khoddam, M.; Hamidon, M.N.B.; Kamsani, N.A.; Rokhani, F.Z.; Shafie, S. Bin An RF Energy Harvester System Using UHF Micropower CMOS Rectifier Based on a Diode Connected CMOS Transistor. *Sci. World J.* **2014**, *2014*, 1–11. [CrossRef] [PubMed]

15. Shameli, A.; Safarian, A.; Rofougaran, A.; Rofougaran, M.; De Flaviis, F. Power Harvester Design for Passive UHF RFID Tag Using a Voltage Boosting Technique. *IEEE Trans. Microw. Theory Tech.* **2007**, *55*, 1089–1097. [CrossRef]

16. Soltani, N.; Yuan, F. A High-Gain Power-Matching Technique for Efficient Radio-Frequency Power Harvest of Passive Wireless Microsystems. *IEEE Trans. Circuits Syst. I Regul. Pap.* **2010**, *57*, 2685–2695. [CrossRef]

17. Curty, J.-P.; Joehl, N.; Krummenacher, F.; Dehollain, C.; Declercq, M.J. A model for u-power rectifier analysis and design. *IEEE Trans. Circuits Syst. I Regul. Pap.* **2005**, *52*, 2771–2779. [CrossRef]

18. Jordana, J.; Reverter, F.; Gasulla, M. Power Efficiency Maximization of an RF Energy Harvester by Fine-tuning an L-matching Network and the Load. *Procedia Eng.* **2015**, *120*, 655–658. [CrossRef]

19. Abouzied, M.A.; Ravichandran, K.; Sanchez-Sinencio, E. A Fully Integrated Reconfigurable Self-Startup RF Energy-Harvesting System With Storage Capability. *IEEE J. Solid-State Circuits* **2017**, *52*, 704–719. [CrossRef]

20. Nimo, A.; Grgić, D.; Reindl, L.M. Optimization of Passive Low Power Wireless Electromagnetic Energy Harvesters. *Sensors* **2012**, *12*, 13636–13663. [CrossRef] [PubMed]

21. Chaour, I.; Fakhfakh, A.; Kanoun, O. Enhanced Passive RF-DC Converter Circuit Efficiency for Low RF Energy Harvesting. *Sensors* **2017**, *17*, 546. [CrossRef] [PubMed]

22. Scorcioni, S.; Larcher, L.; Bertacchini, A. Optimized CMOS RF-DC converters for remote wireless powering of RFID applications. In Proceedings of the 2012 IEEE International Conference on RFID (RFID), Orlando, FL, USA, 3–5 April 2012; IEEE: New York, NY, USA, 2012; pp. 47–53.

23. De Carli, L.G.; Juppa, Y.; Cardoso, A.J.; Galup-Montoro, C.; Schneider, M.C. Maximizing the Power Conversion Efficiency of Ultra-Low-Voltage CMOS Multi-Stage Rectifiers. *IEEE Trans. Circuits Syst. I Regul. Pap.* **2015**, *62*, 967–975. [CrossRef]

24. Soyata, T.; Copeland, L.; Heinzelman, W. RF Energy Harvesting for Embedded Systems: A Survey of Tradeoffs and Methodology. *IEEE Circuits Syst. Mag.* **2016**, *16*, 22–57. [CrossRef]

25. Agrawal, S.; Pandey, S.K.; Singh, J.; Parihar, M.S. Realization of efficient RF energy harvesting circuits employing different matching technique. In Proceedings of the Fifteenth International Symposium on Quality Electronic Design, Santa Clara, CA, USA, 3–5 March 2014; IEEE: New York, NY, USA, 2014; pp. 754–761.

26. Wilas, J.; Jirasereeamornkul, K.; Kumhom, P. Power harvester design for semi-passive UHF RFID Tag using a tunable impedance transformation. In Proceedings of the 2009 9th International Symposium on Communications and Information Technology, Icheon, Korea, 28–30 September 2009; IEEE: New York, NY, USA, 2009; pp. 1441–1445.

27. Lenaerts, B.; Puers, R. *Omnidirectional Inductive Powering for Biomedical Implants. Analog Circuits and Signal Processing*; Springer: New York, NY, USA, 2009.

28. Paing, T.; Shin, J.; Zane, R.; Popovic, Z. Resistor Emulation Approach to Low-Power RF Energy Harvesting. *IEEE Trans. Power Electron.* **2008**, *23*, 1494–1501. [CrossRef]

29. Dolgov, A.; Zane, R.; Popovic, Z. Power Management System for Online Low Power RF Energy Harvesting Optimization. *IEEE Trans. Circuits Syst. I Regul. Pap.* **2010**, *57*, 1802–1811. [CrossRef]

30. Saini, G.; Sarkar, S.; Arrawatia, M.; Baghini, M.S. Efficient power management circuit for RF energy harvesting with 74.27% efficiency at 623nW available power. In Proceedings of the 2016 14th IEEE International New Circuits and Systems Conference (NEWCAS), Vancouver, BC, Canada, 26–29 June 2016; IEEE: New York, NY, USA, 2016; pp. 1–4.

31. Han, Y.; Perreault, D.J. Analysis and Design of High Efficiency Matching Networks. *IEEE Trans. Power Electron.* **2006**, *21*, 1484–1491. [CrossRef]

32. Sun, Y.; Fidler, J.K. Design method for impedance matching networks. *IEEE Proc. Circuits Devices Syst.* **1996**, *143*, 186. [CrossRef]

33. Marian, V.; Allard, B.; Vollaire, C.; Verdier, J. Strategy for Microwave Energy Harvesting From Ambient Field or a Feeding Source. *IEEE Trans. Power Electron.* **2012**, *27*, 4481–4491. [CrossRef]

34. Nimo, A.; Albesa, J.; Reindl, L.M. Investigating the effects of parasitic components on wireless RF energy harvesting. In Proceedings of the 2014 IEEE 11th International Multi-Conference on Systems, Signals & Devices (SSD14), Barcelona, Spain, 11–14 February 2014; IEEE: New York, NY, USA, 2014; pp. 1–6.